REFERENCES

1. J. D. Bierlein and H. Vanherzeele, *J. Opt. Soc. Am. B* **6**, 622 (1989).
2. R. F. Belt, G. Gashurov, and Y. S. Liu, *Laser Focus* **21**, 110 (1985).
3. J. D. Bierlein and C. B. Arweiler, *Appl. Phys. Lett.* **49**, 917 (1986).
4. X. D. Wang, P. Basseras, R. J. D. Miller, J. Sweetser, and I. A. Walmsley, *Opt. Lett.* **15**, 839 (1990).
5. M. Saeed, D. Kim, and L. F. DiMauro, *Appl. Opt.* **29**, 1752 (1990).
6. K. C. Liu and M. G. Cohen, in *Proceedings of Conference on Lasers and Electro-Optics*, Optical Society of America, Baltimore, MD, 24–28 April 1989.
7. A. S. Bechuk, L. A. Kulevskiy, V. V. Smirnov, and Y. N. Solovyeva, *Radio Eng. Electron. Phys. (USSR)* **14**, 919 (1969).

2.B Nonresonant $\chi^{(3)}_{1111}$ Obtained by Nearly Degenerate Four-Wave Mixing Using Chirped-Pulse Technology

Optical nonlinear effects based on the third-order susceptibility $\chi^{(3)}$ are often investigated by four-wave-mixing techniques. Starting with the classic 1965 proof-of-principle experiments by Maker and Terhune,[1] these measurements have yielded $\chi^{(3)}$ values for many condensed compounds. When these measurements are carried out in a fully degenerate manner, i.e., when $\chi^{(3)}_{ijkl}(-\omega, \omega, \omega, -\omega)$ is probed, the experimental hardware requirements become simple and relatively inexpensive, thereby permitting the widespread use of the technique. In a more complicated embodiment using excitation beams of two frequencies, ω_1 and ω_2, and $\omega_1 > \omega_2$, four-wave mixing takes on the form of coherent anti-Stokes Raman scattering (CARS) and coherent Stokes Raman scattering (CSRS), generating new frequencies at either $2\omega_1 - \omega_2$ if intensity $I(\omega_1) >> I(\omega_2)$, or at $2\omega_2 - \omega_1$ if the reverse-intensity condition holds and phase-matching requirements are met. Compared to the fully degenerate case, CARS complicates the measurement by requiring two laser sources and by being sensitive to phase matching. The major strength of this technique is that the output signal is both spatially and spectrally separated from the input beams. Whenever $\chi^{(3)}$ magnitudes are anticipated to be low and thus in need of background-free detection, CARS is the method of choice.

Adair, Chase, and Payne[2] have in recent years adopted a nearly degenerate (near 1.06-μm) version of CARS and derived with it the nonlinear refractive index n_2 for a large number of optical glasses and crystals. In their approach ω_1 is chosen to differ from ω_2 by no more than $\Delta = 60\ cm^{-1}$, thereby simplifying the phase-matching condition for narrow-bandwidth input beams, $\Delta k = \omega/c\ [2n(\omega) - n(\omega + \Delta) - n(\omega - \Delta)]$. The absence of any significant group-velocity dispersion over a 60-cm^{-1} range in all samples considered guarantees an unprotracted, collinear alignment of all input and output beams for $\Delta k \equiv 0$. We report here on nearly degenerate CARS measurements fashioned after those of Adair, Chase, and Payne,[2] using a novel, all-solid-state, single source for generating picosecond pulses at both ω and $\omega - \Delta$.

This approach exploits the spectral pulse-shaping ability of the chirped-pulse-amplification technology[3] (CPA). CPA overcomes the intensity-related *B*-integral effects (self-focusing and damage) that limit the amplification of short picosecond pulses in solid-state lasing media. In CPA, short pulses are temporally stretched because of group velocity dispersion (GVD), amplified to higher energies than could be achieved by amplifying the short pulse directly, and then compressed to a short pulse.

In our laser system[4,5] (shown schematically in Fig. 45.22) 50-ps transform-limited pulses are produced at a rate of 100 MHz in a mode-locked Nd:YLF oscillator. These pulses are fed into a 0.8-km, 9-μm core optical fiber where the pulse undergoes self-phase modulation, increasing the frequency bandwidth[6] to ~40 Å and GVD increasing the pulse length to >100 ps. This pulse is further lengthened by an antiparallel double-pass grating pair. At this point, the ~300-ps pulse is amplified in a Nd:glass regenerative amplifier to an energy of ~1 mJ. This pulse is then recompressed to ~1 ps by a double-pass grating pair[7] made up of 1700-lines/mm, gold-coated, holographic gratings. The bandwidth of the amplified pulse is reduced to ~14 Å by gain narrowing in the regenerative amplifier.

The use of an antiparallel, double-pass pair of gratings allows access to the Fourier transform of the laser pulse (in wavelength space). This allows for spectral pulse shaping by the use of appropriate masks.[8] In our case, we use a hard-edge stop *W* (see Fig. 45.22) to block the central 20 Å of the laser bandwidth. This creates two independent, chirped laser pulses, each with a bandwidth of ~7 Å at ±15 Å from the gain center of the regenerative amplifier. To minimize diffraction effects, a spatial filter before the diffraction gratings is used to place the Fourier transform on a plane exactly at the location of *W*.

These temporally separated pulses are amplified in the regenerative amplifier to an energy of ~0.5 mJ. The symmetry of the injected pulses about the gain center of the regenerative amplifier ensures that the pulses undergo identical amplification and gain narrowing. The resulting pulses each have a bandwidth of 8 Å and are separated by 17 Å.

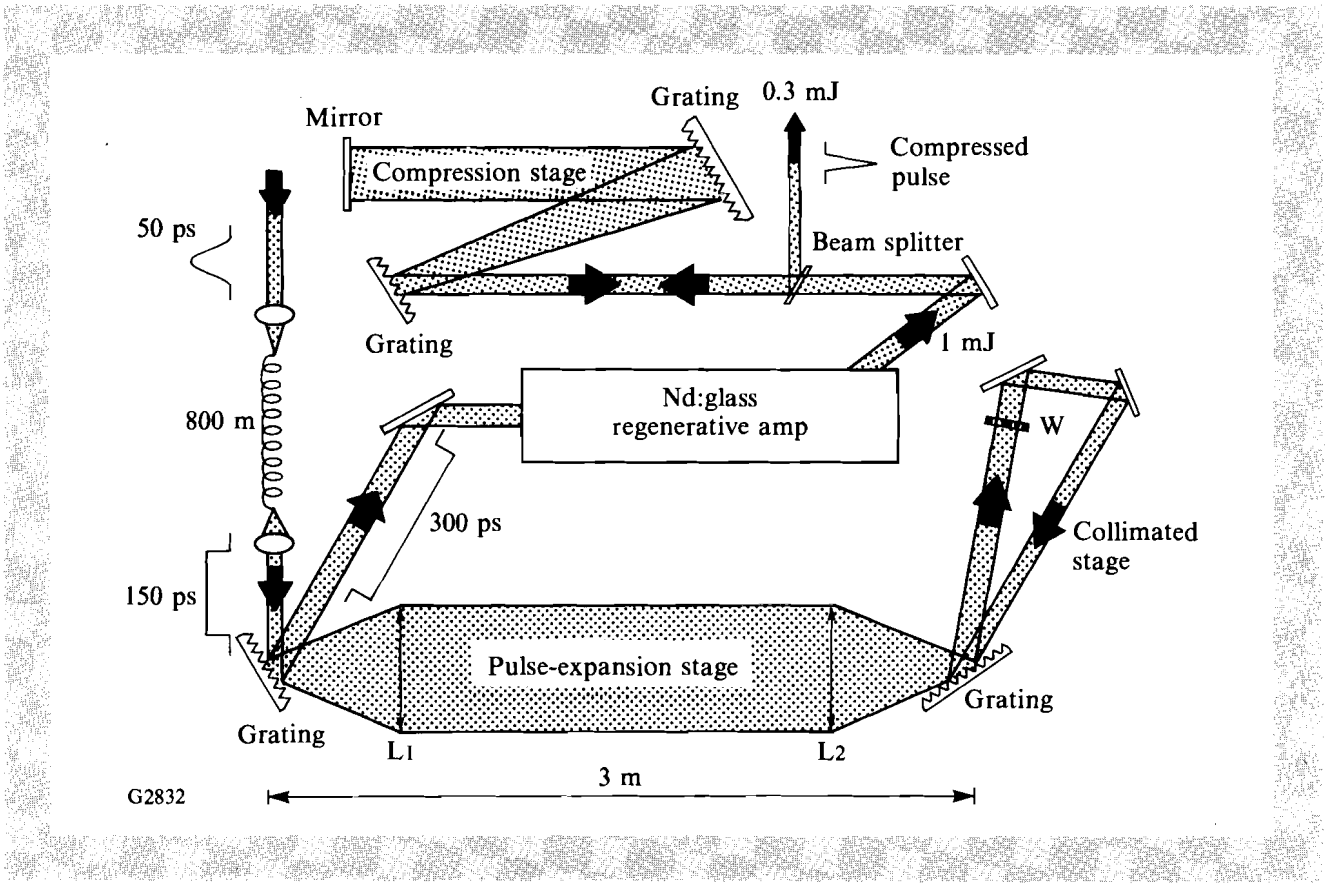

Fig. 45.22
Schematic representation of pulse expansion, spectral windowing, amplification, and pulse compression used in nearly degenerate four-wave-mixing measurements. Using a 50%-output beam splitter after the compression stage can cause feedback into the regenerative amplifier. An improved scheme accomplishes double-pass compression by vertical offset.

Finally, the pulses are spatially filtered and undergo compression in a double-pass, parallel-grating configuration.[7] The autocorrelation of the overlapped pulses is shown in Fig. 45.23. Each of the 75 data points represents a ten-shot average. The 17-Å spectral separation between the two pulses leads to a 2-ps temporal modulation of the combined pulse as expected. This beating must occur for any CARS technique. The envelope of the autocorrelation trace is fitted with a 6.7-ps Gaussian. Because of losses during compression, the pulse reaching the sample carries 0.3-mJ energy.

CARS samples were enclosed in plane-parallel, 0.5-mm-thick cells placed in the converging cone of a 1-m focal-length lens. The beam spot size (0.5 mm) was recorded on calibrated IR film and measured by microdensitometry of the image. The beam exiting the cell, including the $\omega + \Delta$ signal, is recollimated and dispersed by a third double-pass grating pair. The purpose of this grating arrangement is to spatially disperse pump, Stokes, and anti-Stokes signals for a neutral-density filter to attenuate the intense, undepleted signals at ω and $\omega - \Delta$ to about the signal level of the $\omega + \Delta$, four-

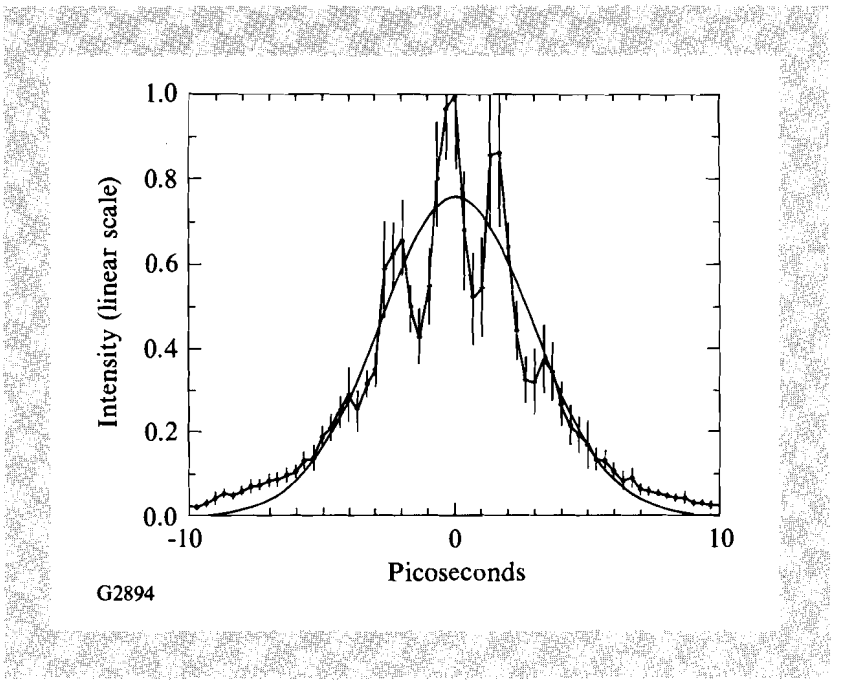

Fig. 45.23
Second-harmonic autocorrelation trace of compressed, spectrally segmented pulse pair. Each data point is a ten-shot average. For comparison, first-order Gaussian (smooth line) is overlayed. The experimentally measured modulation frequency equals the beat frequency between two 17-Å-separated waves.

wave-mixing signal. In this fashion, a cooled, IR-intensified optical multichannel analyzer in the image plane of a monochromator permits recording, within its dynamic-range limits, all signals, $I(\omega)$, $I(\omega - \Delta)$, and $I(\omega + \Delta)$. At the intensity levels prevalent in these measurements, the weaker coherent Stokes four-wave-mixing signal is usually also observed. It appears at $\omega - 2\Delta$ as a result of an interaction of the type $I^2(\omega - \Delta)\, I(\omega)$. Since both $I(\omega)$ and $I(\omega - \Delta)$ have identical polarization, this experiment is probing the tensor component $\chi^{(3)}_{1111}$ of the third-order susceptibility. Figure 45.24 shows the raw-data record of a single-shot measurement on a sample of CS_2.

In Fig. 45.25(a) data show single-shot intensities of the anti-Stokes signal as a function of the pump-intensity product $I^2(\omega)\, I(\omega - \Delta)$ for a 0.5-mm CS_2 path, while those in Fig. 45.25(b) show the coherent Stokes signal plotted against $I^2(\omega - \Delta)\, I(\omega)$. There is a one-to-one correspondence among data pairs in (a) and (b). The single-shot, systematic-measurement error for these data is smaller than the plotted symbols. In assembling Fig. 45.25 only those measurements were selected for which the spectral width at both ω and $\omega - \Delta$ fell within a preselected, spectral interval. Fluctuations in the spectral wings from shot to shot contribute to variations in the degree of compression and in the final, temporal pulse shape. We surmise that the prime source for this spectral-width jitter lies in gain-narrowing effects during amplification of the two pulses by the regenerative amplifier. Over the approximately one-order-of-magnitude intensity range plotted along the abscissa in Figs. 45.25(a) and 45.25(b), one finds the expected linear behavior. The solid lines in Fig. 45.25(a) and 45.25(b) are least-square fits to the data points. The non-zero offset at zero input intensity is attributed to both the CARS and Stokes signals riding on pump-pulse wings that have not been deconvoluted (see Fig. 45.24).

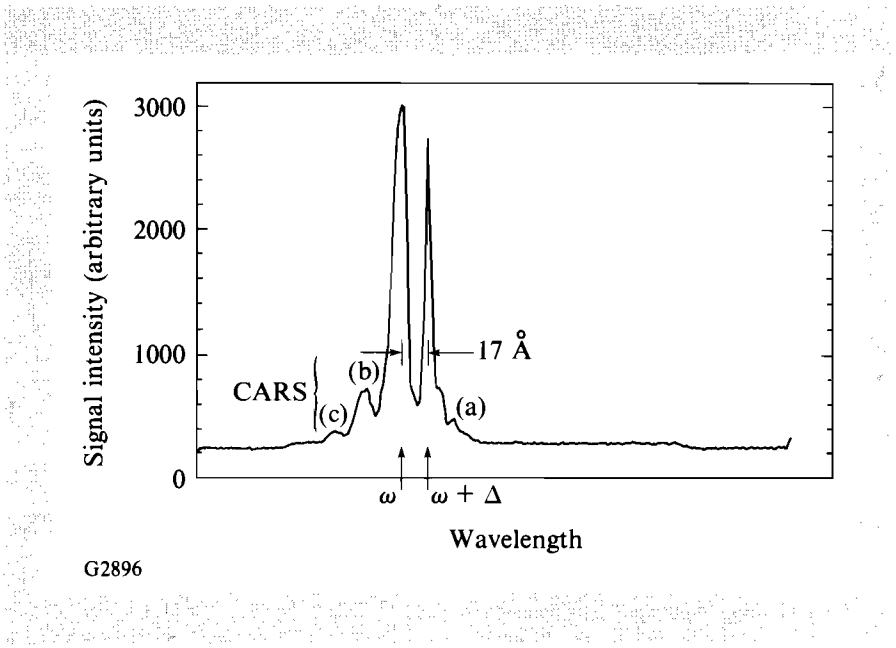

Fig. 45.24
Multichannel detector record from a single-shot, four-wave-mixing event in CS_2. Shorter wavelengths are to the left. The central two peaks represent $I(\omega)$ (left) and $I(\omega + \Delta)$ (right). Clearly resolved are the coherent Stokes (a), anti-Stokes (b), and second-order anti-Stokes (c) peaks.

Monitoring all pertinent intensities $I(\omega)$, $I(\omega - \Delta)$, $I(\omega - 2\Delta)$, and $I(\omega + \Delta)$ on every shot facilitates relative sample-to-sample comparison, recording intensity fluctuations, and checking for pump-intensity depletion by the sample. This complete record permits comparing $\chi^{(3)}$ results from different samples with that of a standard such as CS_2, without the need for irradiating, on each shot, both the sample and the standard. Of course, care must be taken in placing the samples in identical beam positions. In this manner, we measured the relative third-order susceptibility of several organic compounds. Table 45.V lists the relative CARS and coherent Stokes results normalized to CS_2 for nitrobenzene, α-chloronaphthalene, and 4′-octyloxynaphthyl-1′-(4 decyloxybenzoate). In each case the linear refractive index n of the material is accounted for. Refractive indices were measured at 1053 nm on an Abbe refractometer. The last compound is an in-house synthesized liquid crystal out of a series of tolane and ester-linked naphthyl compounds, the nonlinear behavior of which will be published elsewhere. Maintaining alignment throughout the liquid-crystal bulk over the 500-μm sample path was difficult. We chose to measure $\chi^{(3)}$ in the sample's isotropic phase (>90°C), realizing that a penalty in $\chi^{(3)}$ magnitude had to be paid by giving up the macroscopic mesophase alignment. CARS measurements of $\chi^{(3)}$ have been done on liquid-crystalline systems before,[9,10] albeit on different, specific structures. The values for nitrobenzene compare well with the relative value of 0.5 deduced from the 3-ns, four-wave-mixing data of Levenson and Bloembergen.[11] The values for chloronaphthalene can be compared with earlier, relative measurements by Saikan and Marowsky[12]

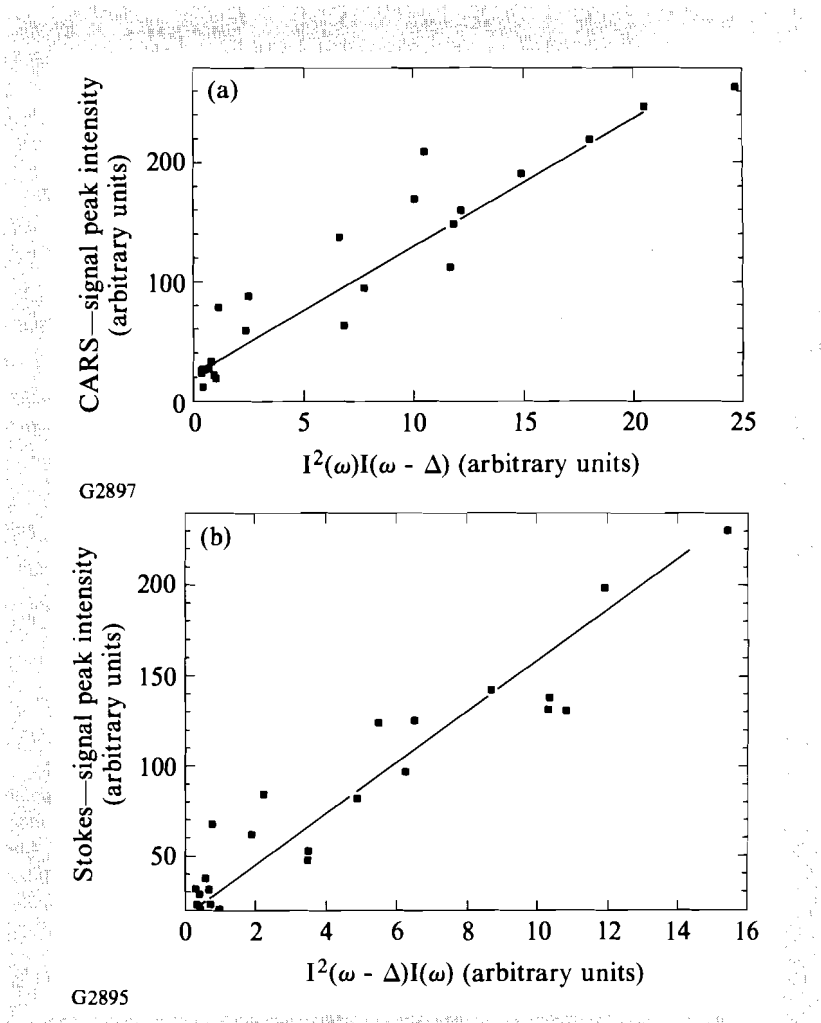

Fig. 45.25
(a) Nonresonant CARS signal magnitude plotted against the input-wave-intensity product $I^2(\omega)I(\omega-\Delta)$. (b) Nonresonant CSRS signal magnitude plotted against the input-wave-intensity product $I^2(\omega-\Delta)I(\omega)$. The data points in (a) and (b) map into each other, i.e., pairs of CARS and CSRS signals were taken simultaneously.

Table 45.V: Measured relative third-order nonlinear susceptibilities $\chi^{(3)}/n^2$.

Material	CS_2	Nitrobenzene	Chloronaphthalene	OONBOB*
CARS	1	0.31±0.07	0.46±0.12	0.37±0.06
CSRS	1	0.29±0.07	0.42±0.10	0.39±0.06
*4′-octyloxynaphthyl-l′-(4 decyloxybenzoate) in isotropic phase				

E5809

who found a relative value of 0.3 for 2-ns excitation near 440 nm. The results show that, within a factor of 2 to 3, these materials approach the $\chi^{(3)}$ values of CS_2.

Finally, we mention that this simple and efficient method for generating both ω and $\omega - \Delta$ allows for several variations. One embodiment takes advantage of the close spectral proximity of Nd emission lines in YAG and YLF (1064 nm versus 1053 nm). By properly synchronizing two, cw mode-locked, Q-switched oscillators[13] one can prepare experimental conditions more elementary than previously described. The major hurdle in this approach is the pulse-to-pulse phase jitter between the two oscillators.[14] Only tight control over jitter assures consistent short-pulse overlap in the sample for acceptable data collection from this third-order nonlinear process. Further experimental simplification can be had by operating a single-gain medium of appropriate bandwidth at two lines simultaneously. In general, any ultrashort pulse source used in conjunction with expansion and compression grating pairs can serve as a driver for this four-wave-mixing experiment.

ACKNOWLEDGMENT

We thank K. Marshall and B. Puchebner for their effort in sample preparation and T. Gunderman for refractive-index measurements.

This work was supported by the U.S. Army Research Office under contract DAAL03-86-K-0173; the U.S. Department of Energy Division of Inertial Fusion under agreement No. DE-FC03-85DP40200 and by the Laser Fusion Feasibility Project at the Laboratory for Laser Energetics, which has the following sponsors: Empire State Electric Energy Research Corporation, New York State Energy Research and Development Authority, Ontario Hydro, and the University of Rochester.

REFERENCES

1. P. D. Maker and R. W. Terhune, *Phys. Rev.* **137**, A801 (1965).
2. R. Adair, L. L. Chase, and S. Payne, *J. Opt. Soc. Am. B* **4**, 875 (1987); R. Adair, L. L. Chase, and S. Payne, *Phys. Rev. B* **5**, 3337 (1989).
3. D. Strickland and G. Mourou, *Opt. Commun.* **56**, 219 (1985).
4. P. Maine, D. Strickland, P. Bado, M. Pessot, and G. Mourou, *IEEE J. Quantum Electron.* **QE-24**, 398 (1988).
5. Y.-H. Chuang, S. Augst, H. Chen, J. Peatross, S. Uchida, and D. Meyerhofer, "Suppression of the Pedestal in a Chirped Pulse Amplification Laser" (submitted to *J. Opt. Soc. Am. B*).
6. D. Grischkowsky and A. C. Balant, *Appl. Phys. Lett.* **41**, 1 (1982).
7. E. B. Treacy, *IEEE J. Quantum Electron.* **QE-5**, 454 (1969).
8. A. M. Weiner, D. E. Leaird, J. S. Patel, and J. R. Wullert, *Opt. Lett.* **15**, 326 (1990).

9. A. F. Bunkin *et al.*, *Vestn. Mosk. Univ. Fiz. Astrom. (USSR)* **18**, 35 (1977).

10. L. S. Aslanyan *et al.*, *Opt. Spectrosc.* **53**, 54 (1982).

11. M. D. Levenson and N. Bloembergen, *J. Chem. Phys.* **60**, 1323 (1974).

12. S. Saikan and G. Marowsky, *Opt. Commun.* **26**, 466 (1978).

13. J. M. Bostick, S. A. Mounter, and C. K. Johnson, *Opt. Commun.* **69**, 54 (1988).

14. For an extensive discussion of oscillator phase jitter, see: M. J. W. Rodwell, D. M. Bloom, and K. J. Weingarten, *IEEE J. Quantum Electron.* **QE-25**, 817 (1989).